

GLAO4ELT: a trade study and SAM experience

A. Tokovinin^a

Cerro Tololo Inter-American Observatory. Casilla 603, La Serena, Chile

Abstract. It is expected that a substantial fraction of wave-front distortions at ELTs will be isoplanatic, being produced jointly by near-ground and dome turbulence, wind buffeting, flexures, and vibrations. We compare various strategies for sensing this "ground" component using (i) several sodium LGSs, (ii) one or several Rayleigh LGSs and (iii) NGSs in a wide field. The experience gained so far with the RLGS GLAO system SAM at 4-m telescope is presented. The results include wide-field partial correction with NGS, vibrations in focus and astigmatism, PSF modeling, and first tests of SAM with UV RLGS.

1 Introduction

Extremely large telescopes (ELTs) gain point-source sensitivity as D^2 from full compensation of turbulence, making the use of Adaptive Optics (AO) a necessity [6]. Indeed, all current ELT projects place heavy emphasis on AO instruments, and two even include deformable mirrors in their main optical train. The attractiveness of partial seeing improvement by ground-layer compensation (GLAO) [5] at ELTs is diminished in comparison with smaller telescopes. Yet, the niche for GLAO still exists. Even a modest improvement in the resolution α pays back because for background-limited imaging and spectroscopy of faint sources the sensitivity is proportional to D/α .

Owing to large apertures and lack of suitably bright laser guide stars (LGSs), full AO correction in the visible at ELTs is not planned. Nevertheless, science programs for ELTs in the optical band (mostly spectroscopy of faint sources) will benefit from seeing improvement by GLAO. The multiplex advantage for multi-object spectroscopy can be exploited by GLAO as well. The field of view (FoV) of ELTs is moderate (20' for GMT), but still too wide to be corrected entirely with AO, especially at short wavelengths.

GLAO can compensate man-made turbulence and vibrations which are expected to be stronger at ELTs because of their larger size (Fig. 1). In this respect GLAO blends with active optics. It can also help diffraction-limited AO systems by offloading fast and/or strong local wavefront distortions, provided that an efficient way of sensing such distortions is in place.

These considerations are not new. In fact all three ELT projects (Table 1) foresee use of GLAO and develop its conceptual designs. In this contribution, we compare alternative wave-front sensing strategies for GLAO and share the experience from one such pathfinder system, SAM.

Table 1. Three ELT designs: FoV and actuator pitch

Project	FoV, '	Adaptive?	d_{act} , m
E-ELT	6	yes	0.5
GMT	20	yes	0.32
TMT	10	no	-

^a atokovinin@ctio.noao.edu

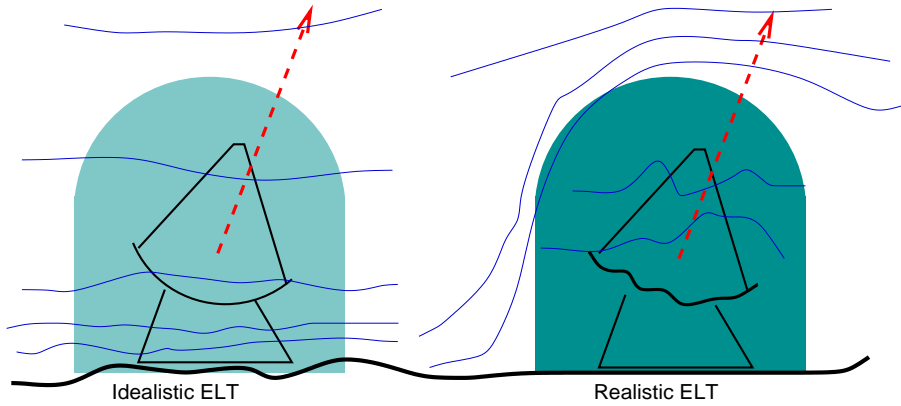


Fig. 1. Illustration of alternative evaluations of surface-layer turbulence in ELT. In the first case, only atmospheric turbulence above the level of primary mirror is considered, as measured in site-testing campaigns, while the ELT is supposed to be “transparent”. This turbulence can be very weak. However, in reality the ELT structure effectively elevates the turbulent surface layer, adds internal turbulence in the dome, and dynamic distortions of the optics. Ubiquitous dome turbulence at existing telescopes is revealed by SCIDARs and SLODARs.

2 Which guide stars for GLAO?

The potential of GLAO depends largely on its ability to correct fast and strong distortions (vibrations, wind buffeting and turbulence) to the highest possible degree (to work in the visible). Fortunately, adaptive mirrors built into the ELTs have rather large actuator density. Getting enough light to drive those mirrors is a problem. Unlike classical AO, seeing improvement does not require small total wavefront residuals, but rather small values of the residual structure function at ~ 1 m baseline [7]. Large but smooth aberrations can be left uncorrected, all that matters is the effective wave-front tilt at 1-m spatial scale.

Three basic choices of guide stars are briefly compared below.

1. Sodium LGS. Multiple sodium LGS for laser tomography are planned by the ELT projects as a baseline for their main AO instruments. Availability of this system made it a logical choice for GLAO. The angle between laser beacons should be made wider for use with GLAO. Yet this solution is not ideal because sodium LGSs are faint, have substantial spot elongation ($\sim 4''$) are not always available owing to laser propagation restrictions (LCH, airplanes, cirrus clouds).

2. Rayleigh LGS will work for GLAO as well, if not better, as sodium LGSs [1]. A ring-like asterism of several RLGSs gives the most uniform correction of the field inside this circle. This mode of operation has been demonstrated at MMT [3]. A single RLGS at low altitude works too; in this case the cone effect discriminates between low and high turbulence and provides crude tomography, as in SAM [8, 10].

Rayleigh lasers are much cheaper than sodium-line lasers. The UV RLGS has been advocated by R. Angel, considering that photon return is proportional to λ^{-3} [2]. This advantage is partially offset by less efficient lasers, optics, and detectors, and by the increased air absorption. The general impression is that doubled and tripled Nd:Yag lasers (532 and 355nm, respectively) give comparable number of return photons per invested dollar. The remaining advantages of the UV RLGS is its invisibility (no airplane hazard) and the ease of separating UV photons from the science beam.

When RLGS are used for laser tomography, they need to be placed as high as possible to sense the whole atmospheric volume. The return signal is proportional to the air density, therefore “high” RLGS call for powerful lasers and/or dynamic refocusing [3]. For GLAO the RLGS height can be much lower. However, spot elongation and field size become important. If we place the RLGS at a short distance H from the telescope, its image is strongly defocused. The angular size of the RLGS footprint at the telescope focal plane equals $\theta = D/H$. This amounts to $10'$ for $H = 10$ km and $D = 30$ m (Fig. 2). If we want to place several RLGSs on a ring, the diameter of this ring must be no more that $7'$ to pass

all laser light through the 20' GMT field. Moreover, the ring projects on different parts of the sky for different aperture segments.

The GMT consists of seven 8.4-m apertures with matching deformable secondary mirrors. For GLAO correction, the individual apertures need not be phased. The focal footprint of RLGS for each aperture is only 3.6', so using one RLGS per aperture may be a good solution.

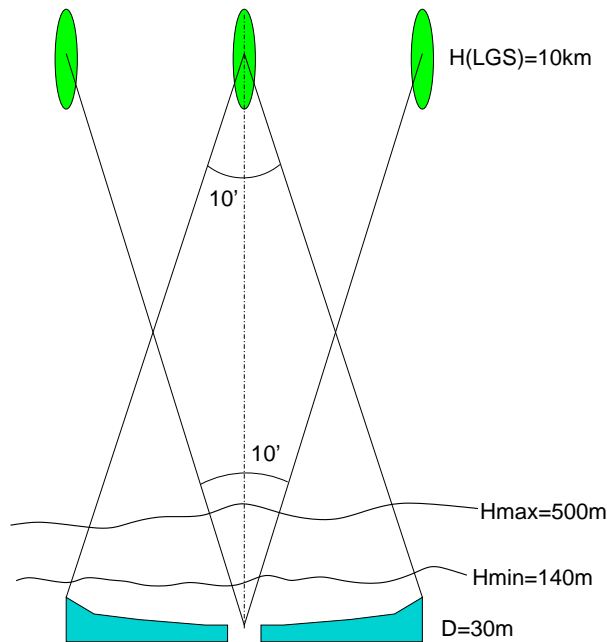


Fig. 2. RLGS geometry. If placed at $H = 10$ km, each LGS covers a $10'$ field in a 30-m telescope. Even larger field is needed for an array of RLGS, this array will project to different directions on the sky for different locations on the aperture. The physical diameter of RLGS “constellation” is comparable to ELT aperture diameter. Turbulence below $H_{\min} = 140$ m will be well corrected in the whole field [7]. Partially sensed turbulence in the “grey zone” up to 500 m (which is usually weak) can cause some anisoplanatism.

3. Natural guide stars (NGS) for wave-front sensing in GLAO seem to be an attractive option. The sky coverage in a small field of classical AO systems is very low, but wider FoV makes things different for GLAO. Selection of several NGS is required anyway with LGS, so why not use them for wave-front sensing? A 20' circular field will contain on average ~ 10 stars of $V = 15^m$ at Galactic pole ($b = 90^\circ$). At $b = 50^\circ$ the GMT field may contain 3 stars of 13^m . Scaling the actual flux in the tip-tilt guide probes of SAM to 0.4-m sub-aperture, we will get ~ 800 el/s from a $V = 15^m$ star. For a wind speed of 4 m/s the sub-aperture crossing time will be 0.1s, requiring a servo bandwidth of ~ 10 Hz. Modern detectors have negligible readout noise, hence the centroid rms error is $\sigma = \sigma_0 N_{\text{ph}}^{-1/2}$, where σ_0 is the rms width of the Gaussian spot, N_{ph} is the number of photons per servo response time. So, the photon noise is simply a $N_{\text{ph}}^{-1/2}$ fraction of the seeing, and with 80 photons the measurement error is 10%. Combination of signals from several NGSs and use of brighter stars further reduce the photon noise. We conclude that a GLAO system based on NGSs can correct slow wavefront distortions at spatial scales comparable to the ELT actuator pitch.

Light from NGSs and science objects cannot be split by wavelength (as in the case of lasers), the only remaining method is to pick up guide stars near the focal plane. In the case of a multi-object spectrometer, robotic positioners can serve for both sensing and science probes. Signals from the NGSs could be combined for tomographic correction of each individual object (MOAO), but low flux will make such option not very interesting because high turbulence is fast. Therefore, the performance of MOAO and GLAO systems based on NGS could be comparable.

4. Combined approach? Rayleigh and natural sources can be used for GLAO in combination, joining their strengths. One on-axis RLGS would give strong flux to sense fast and high-order distortions such as those produced by wind buffeting and vibrations (except tip-tilt). Wavefront correction derived from RLGS is blended with NGS signals to improve uniformity of correction over the field by tomography (better measurement of turbulence in the grey zone). The trade between field size and degree of seeing improvement needs to be addressed, but it may turn out to be irrelevant if most distortions are concentrated below H_{\min} .

3 SAM experience

The SOAR Adaptive Module, SAM [8, 10], is a GLAO system for 4.1-m telescope with a single UV RLGS at $H = 7$ km. The effective actuator pitch is 0.4 m. Unlike most other GLAO systems, SAM is designed to improve seeing at visible wavelengths.

3.1 Tests in the NGS mode

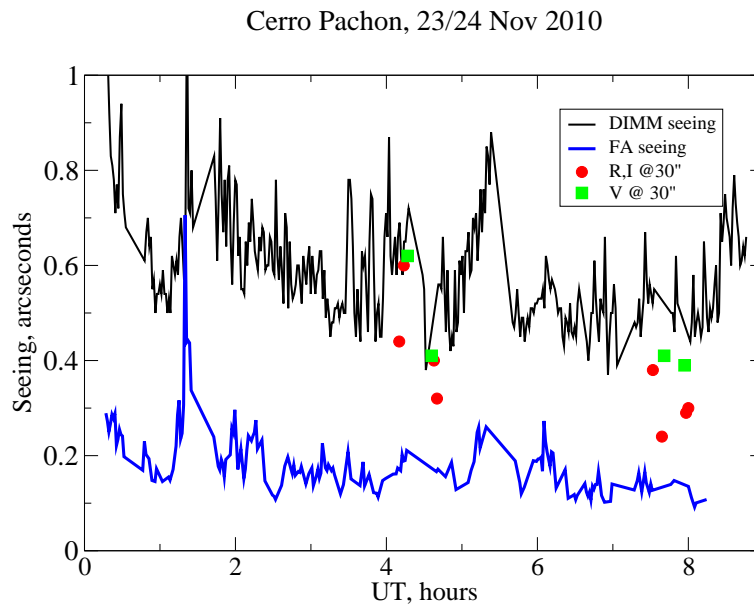


Fig. 3. Seeing evolution on November 23/24 2010 (total, DIMM, and in the free atmosphere, FA). The red circles and green squares mark the FWHM on long-exposure AO-corrected images in the V, R, I bands at $30''$ from the guide star. Observations at airmass of ~ 1.4 , seeing data at zenith.

SAM was tested with the NGS WFS in November 2010 - January 2011. It was a unique combination of an AO instrument with a wide-field visible CCD imager, SAMI (pixel scale 45 mas, FoV $3'$). When the turbulence in the high layers is weak, on-axis correction with just one NGS should improve the “seeing” over the whole field. The correction of high layers is not isoplanatic, but it does not degrade the off-axis resolution substantially because it is small. Such situation indeed happened on November 23, 2010 when the free-atmosphere seeing was below $0.2''$ most of the night (Fig. 3). The FWHM on long-exposure images slowly degraded away from the NGS, but remained better than the seeing over the whole $3'$ field. Figure 4 shows that the non-uniformity and the degree of seeing

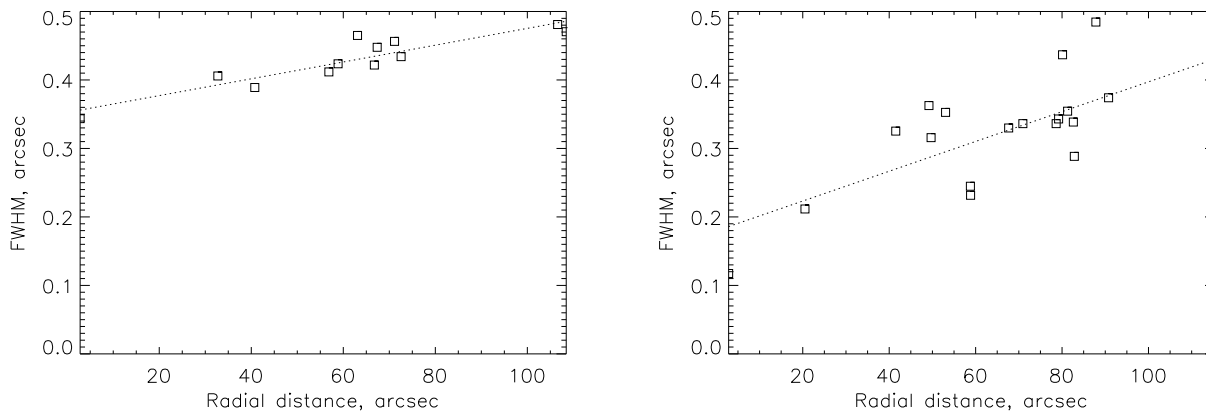


Fig. 4. Dependence of the FWHM resolution on the distance from the guide star. Best data for Nov. 23/24 2010 are plotted. Left: *B*-band, right: *I*-band. Dotted lines are linear fits.

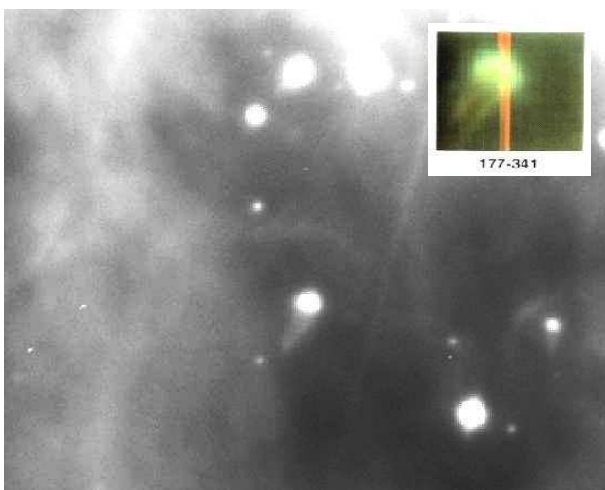


Fig. 5. Fragment of the Orion nebula image in the *R* band recorded with SAM on Nov. 23, 2010. Resolution $\sim 0.40''$, exposure 60s. The proplyd 177-341 and bow-shocks are seen. The insert shows the HST image of this proplyd from O’Dell [4].

improvement are both larger at long wavelengths. Images of the Orion nebula obtained on that night show fine details that were previously seen only with the HST (Fig. 5).

Residual aberrations recorded by the SAM WFS clearly show some vibrations. Tip and tilt have a strong “line” at 50 Hz. Its rms amplitude is not constant: few mas near the zenith and up to 42 mas at low elevations. It is not-stationary in time. We thought previously that the 50-Hz vibration was caused by the SOAR tip-tilt tertiary mirror. In fact it originates in the telescope itself: vibration of the secondary mirror with $1.5 \mu\text{m}$ amplitude is sufficient to explain the 42-mas image jitter at the Cassegrain focus. We also see vibrations in focus (usually at 47 Hz) and in astigmatism (wide peak around 65 Hz), but not in the higher modes (Fig. 6). Most likely, these vibrations are transmitted through the SOAR structure from exciting sources such as motors in the dome or pumps. It is noteworthy that a telescope so small and stiff as SOAR has wave-front distorted by vibrations. A much larger effect is expected at ELTs!

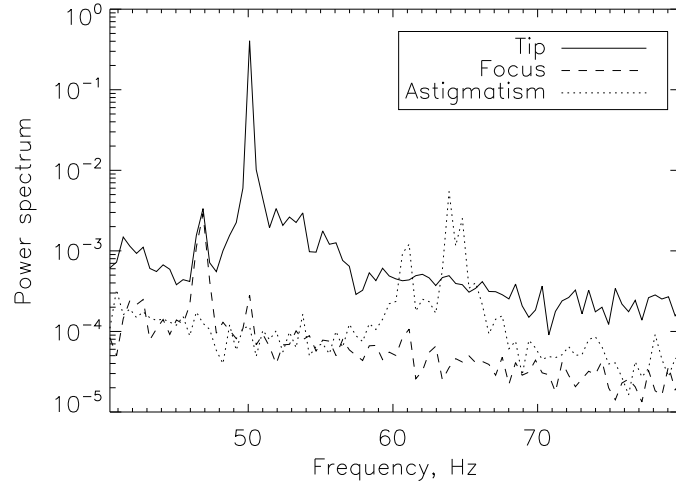


Fig. 6. High-frequency part of the temporal spectra of Zernike modes 2 (tilt, full line), 4 (defocus, dashed line) and 5 (astigmatism, dotted line) recorded with SAM on December 20/21, 2010.

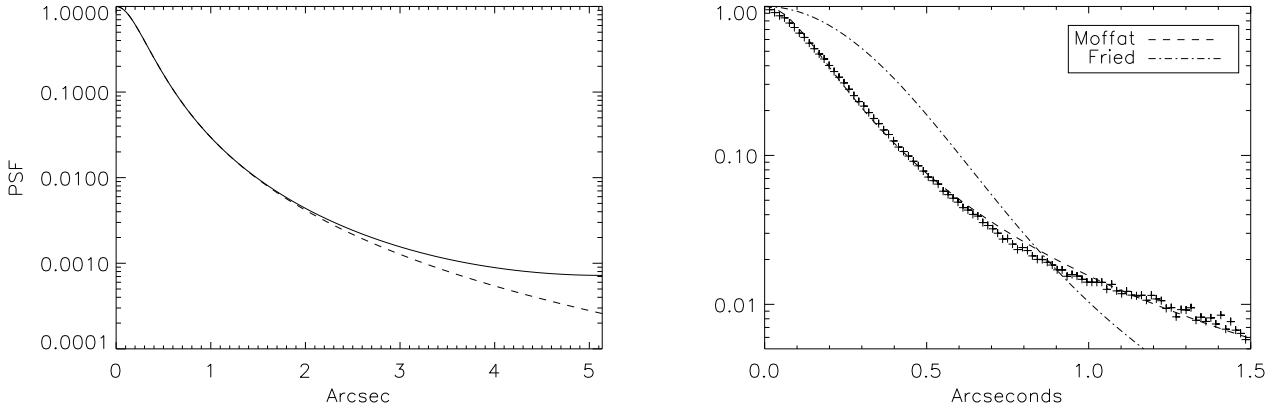


Fig. 7. Left: PSF profile produced by a linear RSF (full line) and its Moffat model (dashed line). Right: radial profile of on-axis SAM PSF in semi-log scale (crosses) and its Moffat model (dashed line, $\beta = 1.22$, y -band, FWHM $0.32''$, seeing $0.62''$). The seeing-limited PSF is plotted in dot-dashed line.

Even without AO correction, the long-exposure seeing-limited PSF has a non-Gaussian profile. Normalized PSF is frequently approximated by the Moffat function

$$I(r) = [1 + (ar)^2]^{-\beta}, \quad (1)$$

where $\text{FWHM} = 2/a \sqrt{2^{1/\beta} - 1}$. A larger β means weaker wings. The case $\beta = 1$ corresponds to the Lorentz profile, while the seeing (Fried) profile is well matched by $\beta = 4.76$.

In the case of SAM, residual errors conspire to produce an almost linear residual structure function (RSF) $E(r) \approx Kr$, where K is the path-length variance in rad^2 at 1 m baseline r [9]. The optical transfer function equals $O(f) = \exp[-0.5(2\pi/\lambda)^2 E(\lambda f)]$. In the 1-dimensional case such negative-exponential OTF corresponds to the Lorentz PSF, $\beta = 1$. In two dimensions, the resulting PSF is well represented by the Moffat profile with $\beta = 1.50$ (Fig. 7, left). Hence, a Moffat PSF with $\beta \sim 1.5$ means a quasi-

linear RSF. A simple scaling law can then be derived

$$FWHM(\lambda) = 0.50'' \frac{\sqrt{E(1\text{m})}}{\lambda} \quad (2)$$

For example, SAM models predict $\sqrt{E(1\text{m})} = 0.4\mu\text{m}$ which leads to $0.40''$ FWHM at $0.5\mu\text{m}$ and $0.29''$ FWHM at $0.7\mu\text{m}$, in general agreement with the actual SAM performance.

The PSFs in SAM indeed resemble this model (Fig. 7, right). Larger β will result from the combination of corrected ground layer and uncorrected high turbulence. The study of GLAO for Gemini [1] indicates that GLAO-corrected PSF in the IR can be fitted by $\beta \sim 2.5$.

3.2 Closing the LGS loop

The SAM instrument was reconfigured into LGS mode in January-March 2011. The LGS loop was first closed on April 14, 2011. During tests on 3 nights, we found that the return flux is polarized when the sky is clear, as expected. The polarization of the emitted beam was adjusted to circular, to reduce flux variations caused by rotating the instrument w.r.t. telescope. With a range gate of $1.5\mu\text{s}$ (225 m) and LGS distance of 7 km , the spot elongation is acceptably small, while the return flux reaches 1500 photons per sub-aperture per 4.3 ms loop cycle. Unfortunately, the LGS spots were still too big, about $2''$. We work on the laser projection optics with a goal to reach sub-arcsecond spot size in the WFS predicted by the model. Until then, the compensation quality and reliability of operation cannot be tested.

We point the LGS by observing un-gated spot with a CCD acquisition camera in the WFS, focused at 7 km . The geometric optics predicts an intensity profile with infinite brightness at center, $I(r) \propto 1/r$. In reality the size of the LGS on the sky is finite, the convolved un-gated profile has finite central brightness and a FWHM some 1.4 times larger than the intrinsic FWHM of the spot. The energy concentration in this case is roughly proportional to the radius, $EE(r) \propto r$, and the slope of this curve gives an estimate of the return flux. Modeling of un-gated LGS images recorded with the SOAR imager in the U filter lead to the total system efficiency (up-link and down-link) of 5% , roughly consistent with the estimates.

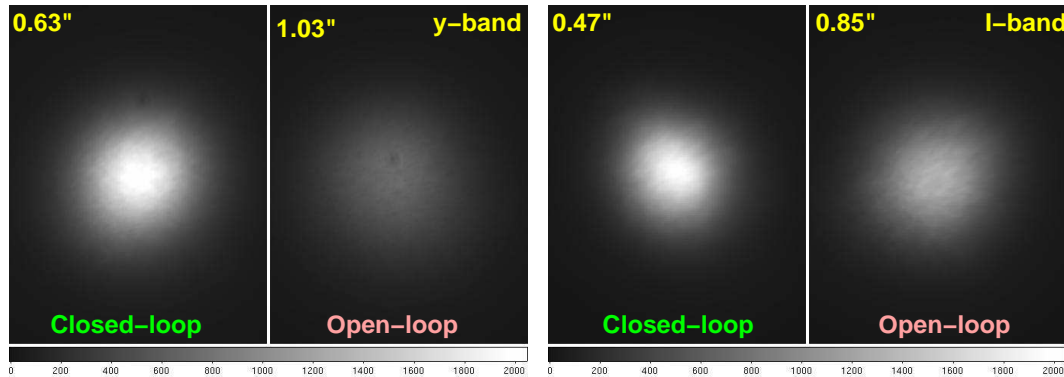


Fig. 8. Images of bright stars recorded on April 15/16 around 2h UT under $0.8''$ seeing. Side-by-side comparison of PSFs in the y band (540 nm , left) and I band (700 nm , right) are shown, with FWHM indicated. The image pairs are displayed on the same spatial and intensity scale.

Figure 8 illustrates partial correction of seeing with SAM on April 15/16, 2011. The instrument was operated in non-optimum conditions (increased noise in the WFS, large spot size). Yet, some gain in the resolution was achieved. These images were obtained by re-centering series of short exposures (we have not used the tip-tilt probes and CCD imager on this occasion). Open-loop data were recorded immediately before or after, with the DM flattened. The thin bimorph DM has substantial flexure

depending on the Nasmyth rotator angle θ . It was compensated in open loop with a look-up table by applying $\sin \theta$ and $\cos \theta$ terms to the voltages of each electrode.

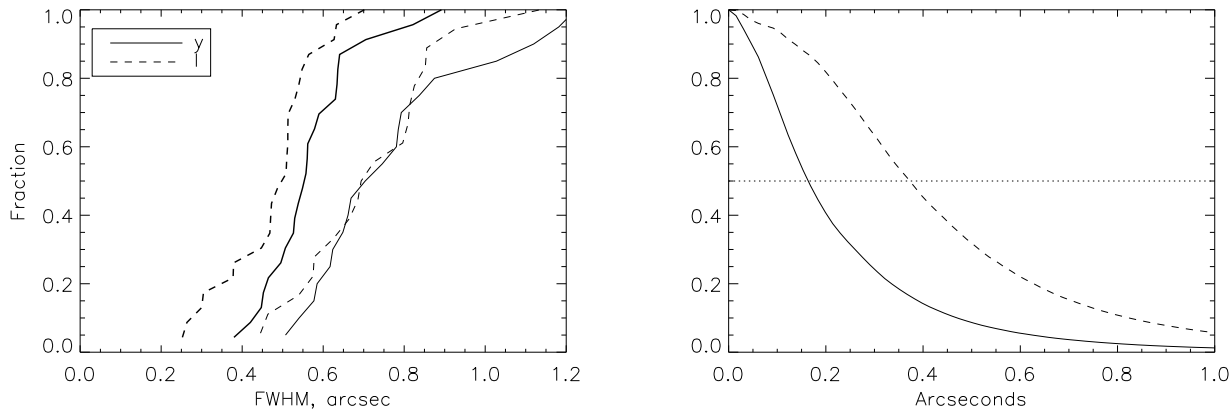


Fig. 9. Left: comparative histograms of FWHM resolution in open (thin lines) and closed (thick lines) loop in two filters. All data for the three nights in April 2011 are used, about 20 measurements per group. Right: radially-averaged PSF profiles for images #115 (CL) and #116 (OL) recorded on April 18/19 around 2h UT and showing the resolution gain in the I band from $0.66''$ to $0.30''$.

The atmospheric conditions on three engineering nights in April were not as exceptional as on November 23, 2010, but the free atmosphere was rather calm. Statistically, the resolution in the closed loop was improved (Fig. 9, left), more in the I filter than in y . The right-hand panel shows PSF of one of the best-compensated images in I recorded with the LGS.

References

1. Andersen, D. R., Stoesz, J., Morris, S. et al. 2006, *PASP*, **118**, 1574
2. Angel, R., Lloyd-Hart, M. *Proc. SPIE*, **4007**, (2000) 270
3. Hart, M., Milton, N. M., Baranec, C. et al. *Nature*, **466**, (2010) 727
4. O'Dell, C. R. *AJ*, **115**, (1998) 2630
5. Rigaut F., in: *Beyond Conventional Adaptive Optics*, Venice, May 2001.
6. Roddier F, ed., *Adaptive optics in astronomy* (Cambridge Univ. Press, Cambridge, 1999).
7. Tokovinin, A. *PASP*, **116**, (2004) 941
8. Tokovinin, A., Gregory, B., Schwarz, H.E. et al. *Proc. SPIE*, **4839**, (2002) 673.
9. Tokovinin, A. *Proc. SPIE*, **7015**, (2008) 77
10. Tokovinin A., Tighe R., Schurter P. et al. *Proc. SPIE*, **7736**, (2010) 132